

Supporting Information

**High-performance Flexible All-Solid-State Aqueous Rechargeable Zn-MnO₂
Microbatteries Integrated with Wearable pressure Sensor**

Bing He^{a,b}, Qichong Zhang^{+b}, Lianhui Li^{+a,b}, Juan Sun^b, Ping Man^{a,b}, Zhenyu Zhou^b, Qiulong Li^b, Jiabin Guo^b, Liyan Xie^{a,b}, Chaowei Li^{a,b}, Xiaona Wang^b, Jingxin Zhao^b, Ting Zhang*^{a,b}
and Yagang Yao*^{a,b}

a. School of Nano Technology and Nano Bionics, University of Science and Technology of China, Hefei, 230026, China

b. Division of Advanced Nanomaterials, Key Laboratory of Nanodevices and Applications, Joint Key Laboratory of Functional Nanomaterials and Devices, CAS Center for Excellence in Nanoscience, Suzhou Institute of Anon-tech and Nano-bionics, Chinese Academy of Sciences, Suzhou 215123, China

[*] Corresponding author. Email: ygyao2013@sinano.ac.cn

tzhang2009@sinano.ac.cn

[+] These authors contribute equally to this work.

1. Materials

Nickel chloride hexahydrate puratrem ($\text{NiCl}_2 \cdot 6\text{H}_2\text{O}$, 98%), sodium acetate ($\text{C}_2\text{H}_3\text{O}_2\text{Na}$, 99%), zinc sulfate heptahydrate ($\text{ZnSO}_4 \cdot 7\text{H}_2\text{O}$), boric acid (H_3BO_3 , 99.8%) and ethanol ($\text{C}_2\text{H}_6\text{O}$, 99.7%) were purchased from Sinopharm Chemical Reagent, China. Hexamethylenetetramine (HMT, $\text{C}_6\text{H}_{12}\text{N}_4$, 99%), sodium sulfate (Na_2SO_4 , 99%), zinc chloride (ZnCl_2 , 98%), lithium chloride (LiCl , 99%), PVA (98.0~99.0%) and manganese sulfate (MnSO_4 , 99%) were provided by Aladdin. CNTF was prepared with a floating catalyst chemical vapor deposition method followed by shrinking with ethanol.

2. Electrochemical Performance Measurements

The electrochemical characterizations of obtained electrode materials was analyzed by cyclic voltammetry curves, galvanostatic charge/discharge curves, and electrochemical impedance spectroscopy measured on an electrochemical workstation (CHI 760E, Chenhua). The electrochemical performance of the aqueous $\text{Ni}@\text{MnO}_2/\text{Zn}$ and MnO_2/Zn batteries was characterized in a two-electrode cell with an aqueous electrolyte containing 2 M ZnCl_2 and 0.4 M MnSO_4 .

3. Characterizations of materials.

The morphologies and microstructures of the electrodes and pressure sensor were analyzed by using a scanning electron microscope (Hitachi S-4800, 5 KV). The crystal structure and chemical composition of samples were characterized by X-ray diffraction (Rigaku D/MAX2500 V) and X-ray photoelectron spectrometer (ESCALab MKII). Transmission electron microscopy images were measured by a high-resolution transmission electron microscope (FEI Tecnai G2 20). The resistance of the pressure sensor was measured by LabVIEW controlled digital source meter (Kethley 2602) and the test voltage was constant 1.5 V.

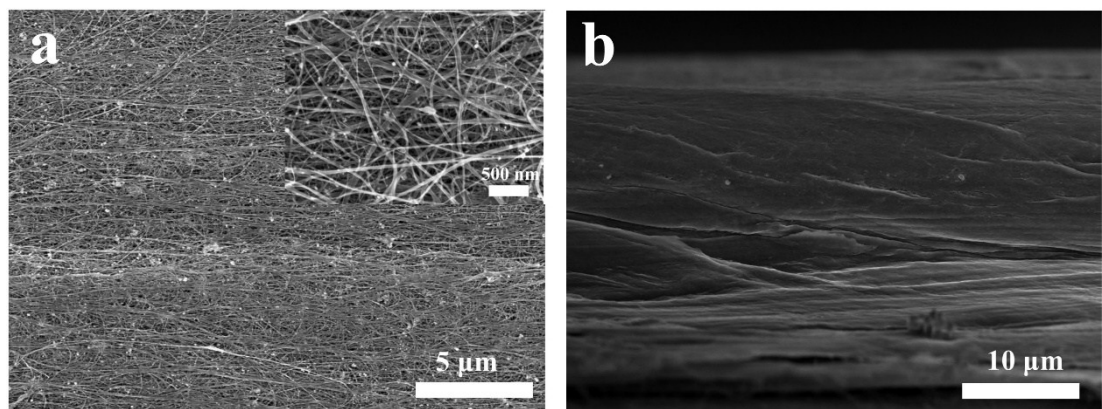


Figure S1 (a) SEM images of the CNTF. (b) Cross-section SEM image of CNTF.

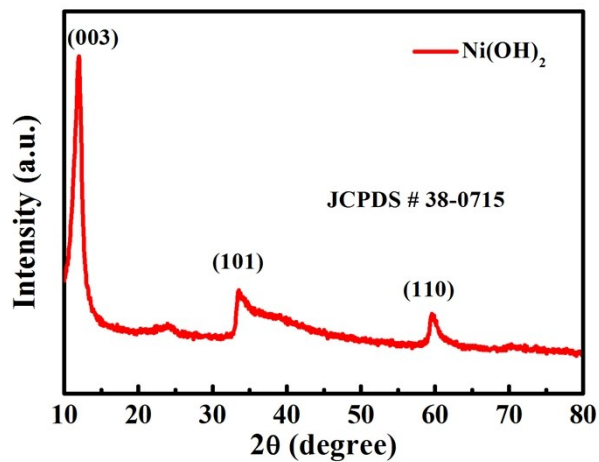


Figure S2 XRD pattern of the Ni(OH)_2 .

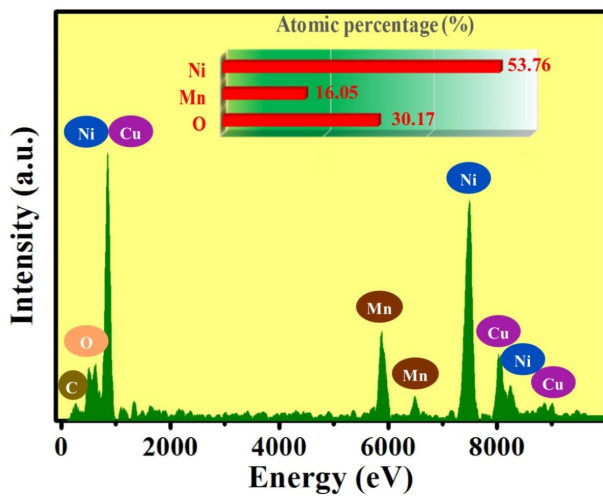


Figure S3 EDS spectrum of 3D CNTF@Ni@MnO₂ core-shell structure.

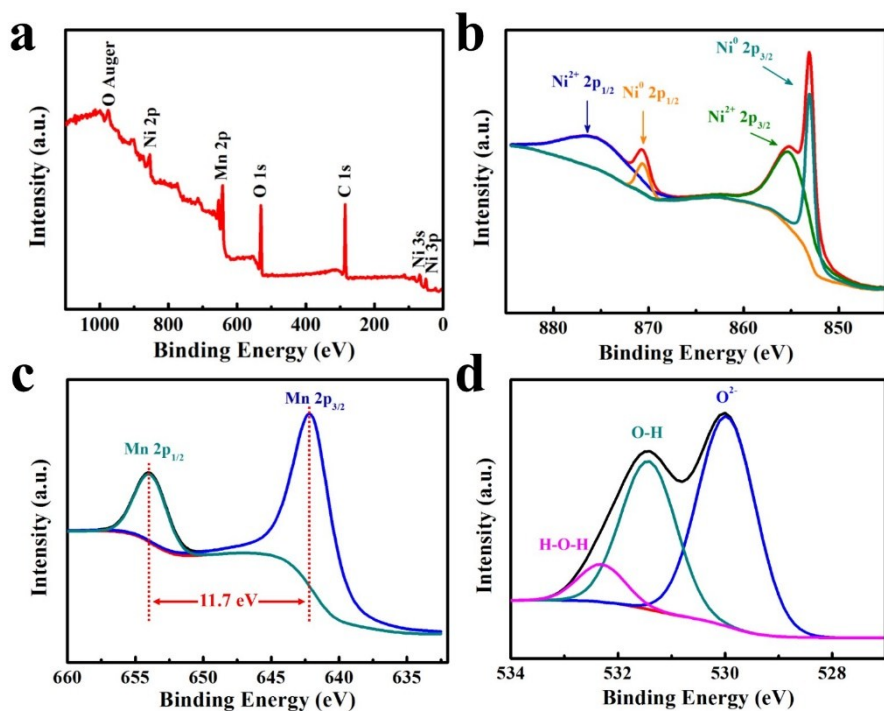


Figure S4 (a) XPS full spectrum of CNTF@Ni@MnO₂, and the deconvoluted Ni 2p (b), Mn 2p (c) and O 1s (d) core level XPS spectra.

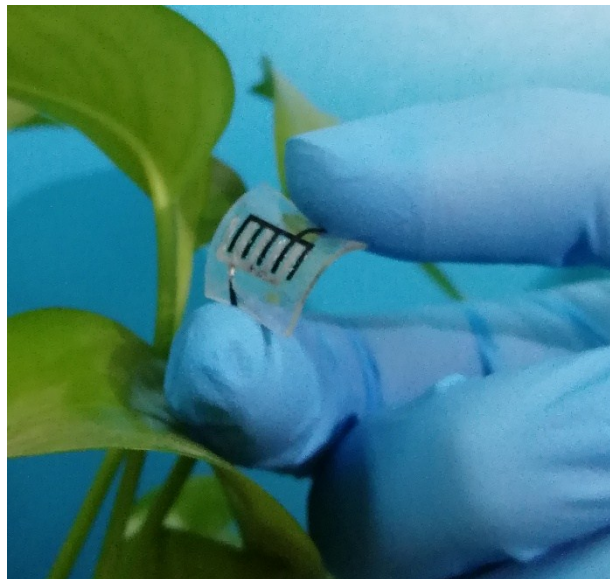


Figure S5 Photograph of the Ni@MnO₂//Zn microbattery.

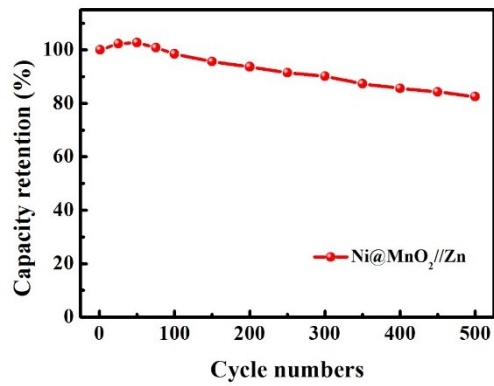


Figure S6 Cycling performance of the all-solid-state Ni@MnO₂//Zn microbatteries with at a current density of 0.1 mA cm⁻².

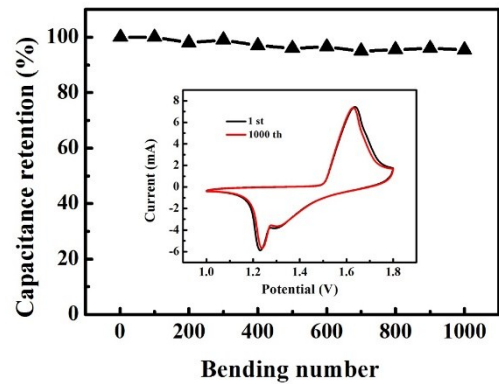


Figure S7 Bending performance of the all-solid-state Ni@MnO₂//Zn microbattery at a current density of 0.1 mA cm⁻².

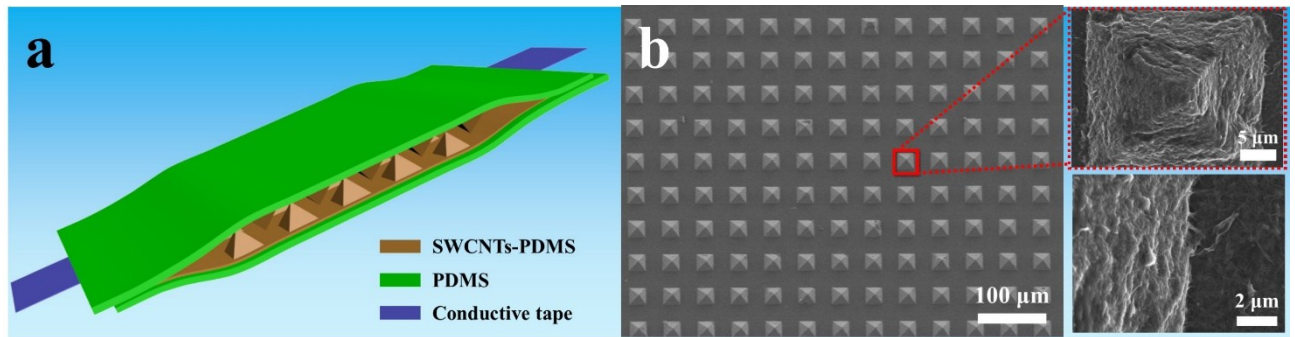


Figure S8 (a) Schematic diagram of the pressure sensor. (b) SEM image showing the micro-patterned surface of the PDMS.

The pressure sensor was constructed using two SWCNTs–PDMS bilayers (SPP) with the micro-patterned surfaces touching each other and the microbattery was assembled on the other side of the PDMS substrate, as schematically shown in Figure S8a. The SWCNTs were used as the conductive network layer for their high conductivity, flexibility, and stability. The SEM image of the top view of SPP shows that the SCWNTs network was tightly and uniformly embedded in the pyramid micro-structures and the interspace between the micro-structures (Fig S8b), which was ascribed to the etching of Dimethyl Formamide (DMF) for PDMS and the pyrolysis of PDMS in the process of spraying under high temperature.

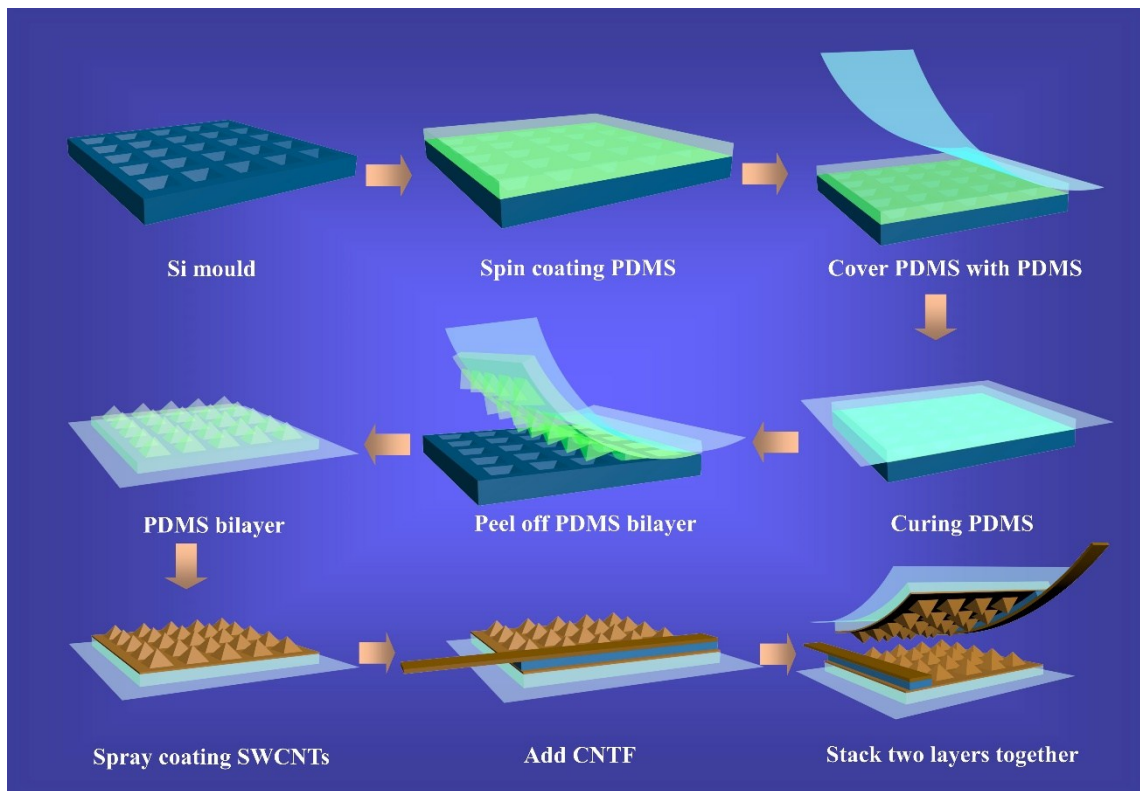


Figure S9 Schematic of fabricating process to the strain sensor.

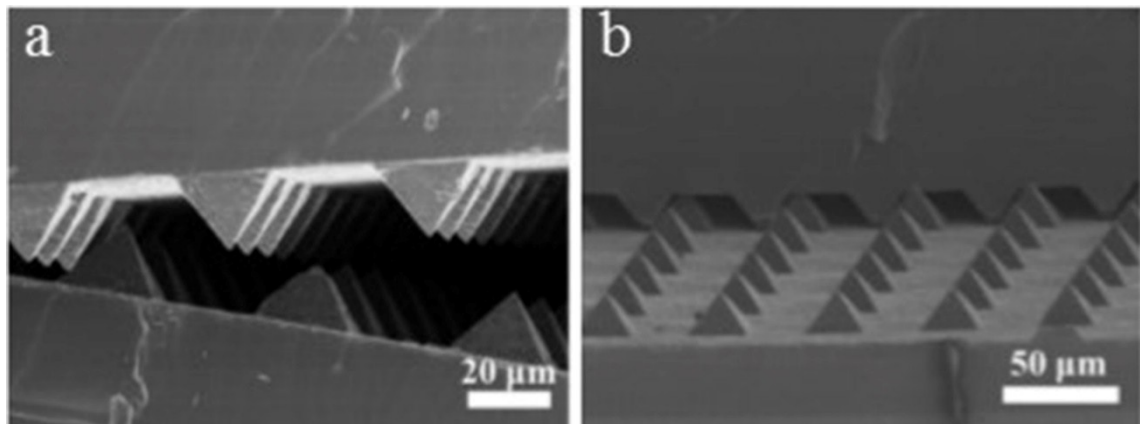


Figure S10 Side view SEM image of the pressure sensor: the relaxed state (a); stress state (b).

Side view SEM image (Figure S10) exhibits the stress procedure of the pressure sensor: when the sensor is in relaxed state, only a few parts of the two sensitive layers contact and there is an obvious air gap between them resulting in a considerable resistance of the sensor in that state. Once the sensors suffer stress, the contact point of the two SWNTs–PDMS (SPP) bilayers with the micro-patterned surfaces begins to increase and the greater the force, the greater the contact area.

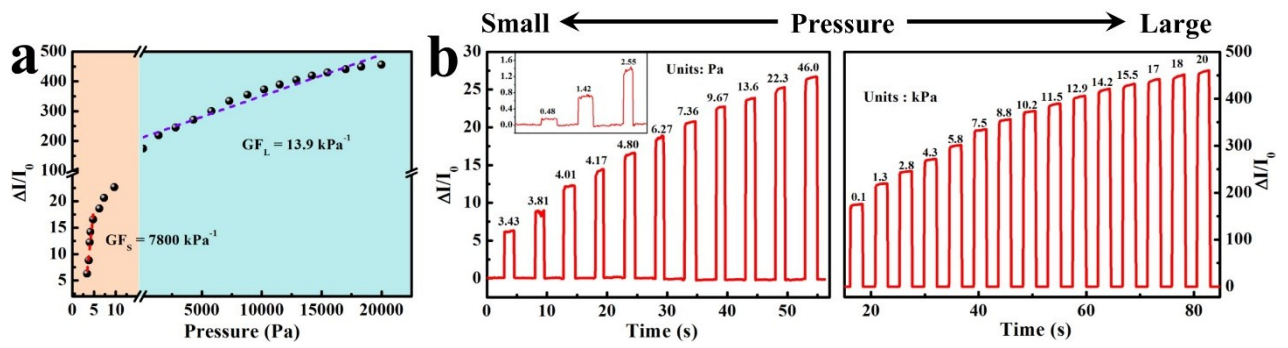


Figure S11 (a) Relative current change as a function of pressure. (b) Real-time response of the strain sensor to different pressure. Left: Real-time response of the pressure sensor to small pressure range. Right: Real-time response of the pressure sensor to large pressure range.

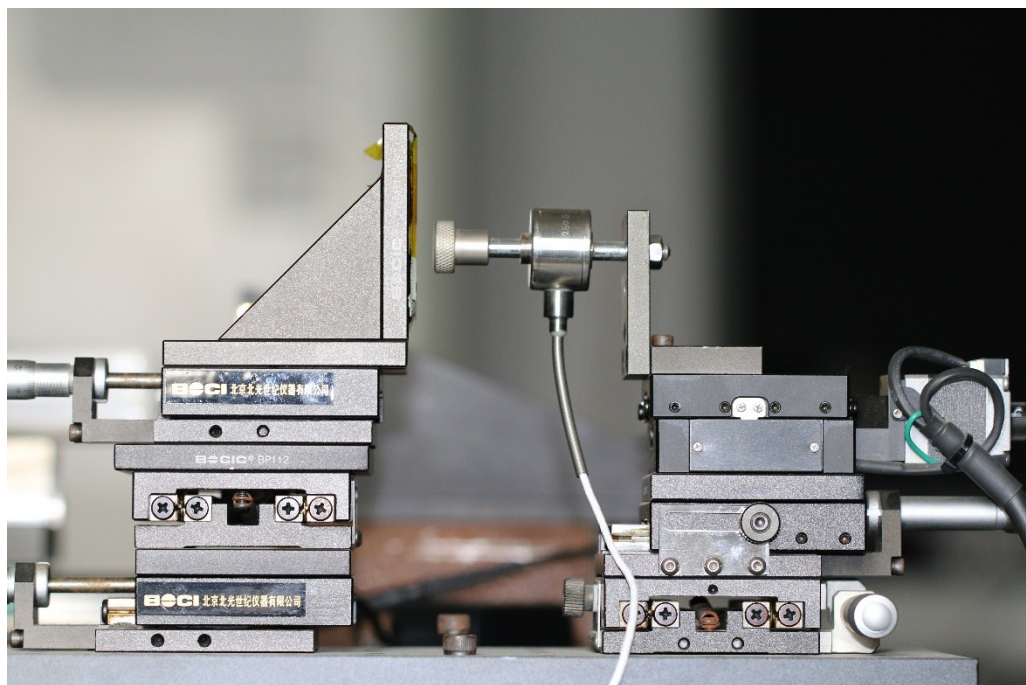


Figure S12 Photograph of commercial force gauge (Aliyiqi HF-2N) stepper machine system.

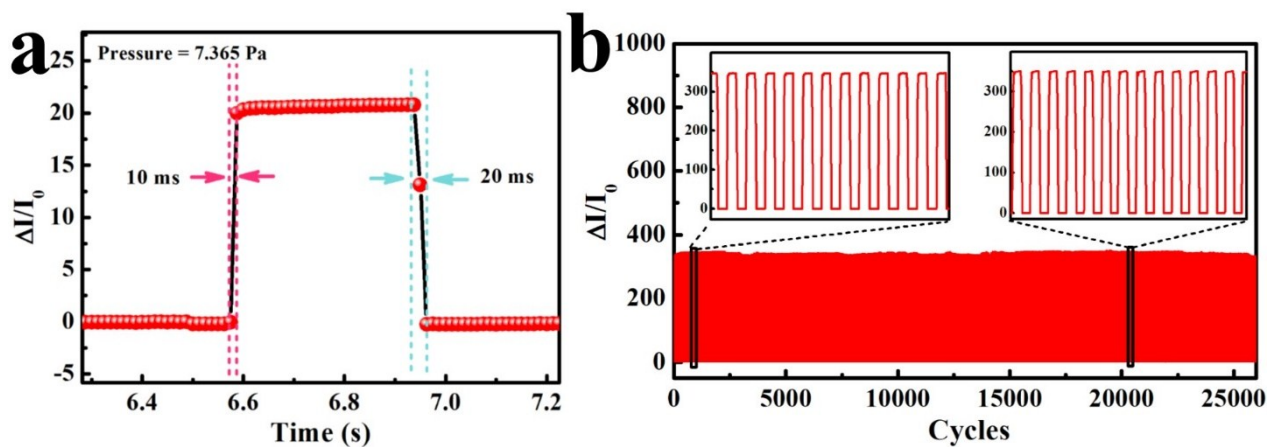


Figure S13 (a) Time response of the pressure sensor upon applying a quasi-transient step 7.365 Pa pressure. (b) Relative current variation under cyclic pressure from 0 Pa to 7.5 kPa with a frequency of 0.5 Hz over 26000 cycles. The sensor was powered by digital source meter (Kethley 2602) with 1.5V.



Figure S14 Photograph of integrated device thickness measure.